1227

NASA Technical Memorandum 87306

Beam-Modulation Methods in Quantitative and Flow-Visualization Holographic Interferometry

Arthur J. Decker
Lewis Research Center
Cleveland, Ohio

Prepared for the
Advanced Instrumentation for Aero Engine Components
sponsored by AGARD
Philadelphia, Pennsylvania, May 19–23, 1986

NASA

BEAM-MODULATION METHODS IN QUANTITATIVE AND FLOW-VISUALIZATION HOLOGRAPHIC INTERFEROMETRY

Arthur J. Decker
National Aeronautics and Space Administration
Lewis Research Center
Cleveland, Ohio 44135

SUMMARY

This report discusses heterodyne holographic interferometry and time-average holography with a frequency shifted reference beam. Both methods will be used for the measurement and visualization of internal transonic flows, where the target facility is a flutter cascade. The background and experimental requirements for both methods are reviewed. Measurements using heterodyne holographic interferometry are presented. The performance of the laser required for time-average holography of time-varying transonic flows is discussed.

INTRODUCTION

Among the beam-modulation methods described in the literature are diffuse-illumination heterodyne holographic interfereometry[1-4] and diffuse-illumination time-average holography with frequency modulation of the reference wave.[5-7] A goal at NASA Lewis Research Center is to implement both methods in a test-cell environment as well as in the laboratory. The intended applications are structural analysis, flow visualization, and flow-properties measurements.

The technological problems and details that must be attended to for these methods are similar for structural analysis and for the measurement or visualization of internal transonic flows. This paper, then, centers on internal transonic flows, although we are by no means exclusively or even primarily interested in this flow region. A major factor is that a number of transonic-flow facilities have been constructed in the past decade.[8-12] Some of these facilities are available for evaluating heterodyne and time-average holography. The degree of difficulty is realistic: techniques which have some successes in the internal transonic environment are likely to be transferable to other applications in the field. One particular facility, a flutter cascade of blades vibrating in a pitching motion, has been tested with schlieren,[11] rainbow schlieren,[13] and holographic flow visualization,[14] and is convenient for a test of the beam modulation methods.

Some difficulties in implementing diffuse-illumination, heterodyne, holographic interferometry for flow measurements are generation of the two reference beams required and transference of alignment from the test-cell to the hologram readout station. Other difficulties are the generation of a fringe pattern with enough contrast or signal-to-noise, and the avoidance of time-varying fringe patterns produced by components other than the flow.

A major incentive for overcoming these difficulties is that the necessary hardware for both methods is available off-the-shelf, with minimal modifications. For the heterodyne techniques, this hardware includes pulsed lasers with interpulse beam-switching capability, stable continuous wave lasers, acoustooptic frequency shifters, and inexpensive computers and computer controlled accessories.

The major difficulty in implementing time-average holography for flow visualization is the acquisition of a suitable laser system. For time-average holography, there is at least one long-pulse flashlamp-pumped dye laser with good beam uniformity, which requires some modifications for the holographic application. This laser is being acquired for evaluation, since it offers the combination of energy and pulse length required for transonic flow visualization.

The available hardware makes it possible and desirable to take advantage of some well known properties of heterodyne and time-average holographic interferometry. Included are the high precision, the continuous fringe interpolation capability, and the computer compatibility of heterodyne interferometry, and the fringe-contrast control capability of time-average holography. These properties are combined with the advantages and disadvantages of diffuse-illumination interferometry, including the fringe-localization effect, three-dimensional measurements and visualization, and the noise of the laser speckle effect.

This paper summarizes some steps taken and conclusions arrived at in the NASA Lewis program. A general background for beam modulation methods is presented: diffuse-illumination heterodyne and time-average holography are two special cases. Then the quantitative fundamentals of these two special cases are reviewed, and the status of the implementation of these cases is discussed in terms of hardware, tests, experimental results, and future potential.

BACKGROUND

Most of the concepts of holographic optical processing of the past 24 years can be represented by two equations. At the recording plane H of a two-dimensional hologram, the reconstructed wave satisfies the proportionality

$$O_R(r_H,t) \propto \int S(r_H,t')O(r_H,t')R^*(r_H,t')R_R(r_H,t)\,dt' \tag{1}$$

where

$O(r_H,t)$ is the object wave,

$R(r_H,t)$ is the reference wave,

$R_R(r_H,t)$ is the reconstruction wave,

and $S(r_H,t)$ is the shutter function, which can be absorbed mathematically in the reference wave. The position on the hologram is denoted by r_H, and all functions potentially have a relative time dependence denoted by t.

A second equation is obtained by including linear operations preceding and following the hologram recording step. If an object wave $O_O(r_O,t)$ originates at positions r_O and a reconstructed wave $O_R(r_D,t)$ is subsequently detected at positions r_D, then

$$O_R(r_D,t) \propto \iiiiint h_R(r_D;r_H;t;t_H)h(r_H;r_O;t_H';t_O)O_O(r_O,t_O) R^*(r_H,t_H')R_R(r_H,t_H)\,dt_H\,dr_H\,dt_H'\,dt_O\,dr_O \tag{2}$$

where h_R and h are impulse response functions connecting the detection (r_D,t), the reconstruction (r_H,t_H), the recording (r_H,t_H'), and the object (r_O,t_O) coordinates and times.

The selections of R and R_R can be used to enhance the visualization of the object wave O_O, or to condition the object wave for measurements and analysis.

For methods discussed in this paper, R and R_R are carefully matched geometrically, so as to faithfully reconstruct the object wave fronts. The form of the output wave O_R is determined by time modulation of R and R_R. Diffuse-illumination holography is used exclusively, and the usual geometrical optics viewpoint is adopted. The consequences of these choices are summarized next.

Diffuse-Illumination Interferometry[15]

In diffuse-illumination holography, light rays arrive at each point r_H at the hologram recording plane from all parts of the fluid. For linear recording, the light rays are treated independently. Associated with the direction of polarization of the reference wave, each light ray has a magnitude and a phase, where the phase has both a random and a deterministic part. For a time-varying fluid, the deterministic part has a time variation apart from the variation at the frequency of light. The impulse-response functions in Eq. (2) are associated with the propagation and imaging of light rays, and need not be mentioned again. Where different light rays intersect, the random component of phase leads to a high frequency interference effect called the laser speckle effect. Within a given light ray, the time variation of phase is given by a familiar expression

$$\phi(t) = \frac{2\pi}{\lambda} G \int_{S_1}^{S_2} \rho(r,t)\,dS \tag{3}$$

where λ is the wavelength of the laser beam, G is the Gladstone-Dale coefficient ($G = 0.227\times10^{-3}$ m^3/kg for air at $\lambda = 532$ nm), $\rho(r,t)$ is the density as a function of position on the light ray r and the time t, and S is the distance along the light ray.

The light rays themselves are generally curved lines, but, for the internal-flow facilities treated herein, it is reasonable to assume that the rays are straight lines (refractionless limit).[16,17] A fringe pattern is formed as in Fig. 1, when the light rays are superimposed by imaging. Except for explaining the speckle effect, the intensities of the individual light rays add independently, so that the interference pattern I is given by the proportionality.

$$I \propto \sum_i I_{1i} + \sum_i I_{2i} \cos(\Delta\phi_i) \tag{4}$$

where i is a ray-to-ray summation index, carried over an imaging pencil, and $\Delta\phi_i$ is the phase relative to a reference.

The fringe pattern will have high contrast only for those images of points where the variation of $\Delta\phi_i$ is negligible within the imaging pencil. Then, a first-order criterion for high contrast is the fringe localization condition

$$\partial\Delta\phi/\partial\theta_{ix} = 0 \qquad \partial\Delta\phi/\partial\theta_{iy} = 0 \tag{5}$$

where θ_{ix} and θ_{iy} are angles about the central ray z in the xz and yz planes, respectively (Fig. 1). When θ_{ix} and θ_{iy} are not independent as in slit viewing, a single localization equation applies.

Equations (4) and (5) imply that each point in a high-contrast fringe pattern can be associated with the central ray of the imaging pencil. The intensity is determined by the interferometric phase for that ray as given by Eq. (3). For some flow features such as shock-wave surfaces,[14,18-19] Eq. (5) predicts that localization will occur nearby, on, or within the flow feature, thereby providing three-dimensional visualization of the flow feature.

Double-exposure techniques for performing measurements or visualization based on Eqs. (1) to (5) are reviewed next.

Double-Exposure Techniques

Ordinary double-exposure holographic interferometry, heterodyne holographic interferometry, and quasi-heterodyne holographic interferometry are derivable from Eq. (1). In all cases, individual exposures are short when compared with the time variation of $\Delta\phi$. Then the shutter function is represented by the proportionality

$$S(r_H,t) \propto \delta(t) + \delta(t-T) \tag{6}$$

where T is the time between exposures, and the reconstructed ray is represented by the proportionality

$$O_R(r_H,t) \propto O(r_H,0)R^*(r_H,0)R_R(r_H,t) + O(r_H,T)R^*(r_H,T)R_R(r_H,t) \tag{7}$$

In Eq. (7), the phase difference between exposures (interference phase) is given by

$$\Delta\phi = \frac{2\pi}{\lambda} G \int [\rho(r_H,T) - \rho(r_H,0)]\, dS \tag{8}$$

and the interference pattern is of course proportional to

$$/O_R(r_H,t)/^2$$

For a faithful reconstruction of the geometry of a light ray, the reconstruction wave has the form

$$R_R(r_H,T) = R(r_H,0) \exp [j(\gamma_0(r_H) + \omega_o t)] + R(r_H,T) \exp [j(\gamma_T(r_H) + \omega_T t)] \tag{9}$$

where the γ's are phase shifts and the ω's are circular light frequencies. That is, the reference wave at each of the two exposures is matched by one term of the reconstruction wave, except possibly for a small phase shift and a frequency offset.

For ordinary double-exposure holography, the geometry and time-independent phase of the reference do not change between exposures and are matched during reconstruction.

$$R(r_H,0) = R(r_H,T)$$

$$\gamma_0(r_H) = \gamma_T(r_H)$$

$$\omega_T = \omega_0$$

The interference pattern has the general form

$$I = I_1 + I_2 \cos(\Delta\phi) \tag{10}$$

where the interference phase is given by Eq. (8).

For the heterodyne techniques, the reference beams are geometrically distinct at the two exposures.

Then, for heterodyne holographic interferometry,

$$R(r_H,0) \neq R(r_H,T)$$

$$\gamma_0(r_H) = \gamma_T(r_H)$$

$$\omega_0 \neq \omega_T$$

and the interference pattern assumes the time varying form

$$I = I_1 + I_2 \cos[\Delta\phi + (\omega_T - \omega_0)t] \tag{11}$$

The interference phase can be measured relative to a reference by using a phase sensitive detector.

For quasi-heterodyne holographic interferometry,

$$R(r_H,0) \neq R(r_H,T)$$

$$\gamma_0(r_H) \neq \gamma_T(r_H)$$

$$\omega_0 = \omega_T$$

and the interference pattern has the form

$$I = I_1 + I_2 \cos[\Delta\phi + \gamma_T(r_H) - \gamma_0(r_H)] \tag{12}$$

If $\Delta\gamma(r_H)$ is given three different values, typically 0, 120, and 240°, and if I is measured at each value, then the interference phase is given by

$$\Delta\phi = \tan^{-1}\left[\frac{\sqrt{3}\,(I_{240} - I_{120})}{(2I_0 - I_{120} - I_{240})}\right] \tag{13}$$

It is also to be noted that the choice of $\Delta\gamma(r_H)$ can be used to modify or control fringe contrast and fringe localization. Equation (5) assumes the modified form

$$\begin{aligned} \partial[\Delta\phi(r_H) + \Delta\gamma(r_H)]/\partial\theta_{ix} &= 0 \\ \partial[\Delta\phi(r_H) + \Delta\gamma(r_H)]/\partial\theta_{iy} &= 0 \end{aligned} \tag{14}$$

In this paper, the modification of fringe contrast is left to time-average holography, the next topic for review.

Time-Average Holography[20]

For time-average holography, the reference and reconstruction beams are geometrically identical. The reference wave may have a relative time dependence. For an exposure time T, the reconstructed wave from Eq. (1) is given by the proportionality

$$O_R(r_H) \propto \int_0^T O(r_H,t')/R(r_H)/^2 \exp[-j\gamma(r_H,t')]\,dt' \tag{15}$$

where $\gamma(r_H,t)$ represents the relative time dependence of the phase of the reference wave. In terms of the time varying phases of the reference and object waves, the reconstructed wave satisfies the proportionally

$$O_R(r_H) \propto \int_0^T \exp[j(\Delta\phi(r_H,t') - \gamma(r_H,t'))]\,dt' \tag{16}$$

Time-average analysis is easiest when the time and position dependences of the phases can be separated.[20] To first order for a flow, that separation assumes the form

$$\Delta\phi(r_H,t) = t\phi_r(r_H) \tag{17}$$

If the time dependence of the reference wave is chosen to have the same form, then

$$\gamma(r_H,t) = t\gamma_r(r_H) \tag{18}$$

For these time dependences, Eq. (16) reduces to

$$O_R \propto \frac{T\sin[(\phi_r(r_H) - \gamma_r(r_H))T/2]}{[(\phi_r(r_H) - \gamma_r(r_H))T/2]} \tag{19}$$

A brightest fringe will occur when $\phi_r - \gamma_r = 0$, where $\gamma_r(r_H)$ is a simple shift in the circular frequency of the reference wave. Hence, for flow visualization, the highest contrast can be chosen for the flow-feature of interest, by the correct choice of a frequency offset of the reference wave.

IMPLEMENTATION OF HETERODYNE HOLOGRAPHIC INTERFEROMETRY

Objective and Requirements

The eventual objective is to perform heterodyne diffuse-illumination holographic interferometry in a nine-blade transonic flutter cascade. The blades in this machine are vibrated about their midchord axes to simulate aeroelastic instability or flutter.[11] The density field is time dependent as a result of this motion. Holographic flow visualization has been performed in this cascade, and its performance for holography has been well documented.[14]

The flutter cascade is a fairly difficult test rig for performing holographic interferometry, and any positive results would be encouraging. Diffuse-illumination holographic interferometry is performed by shining a laser beam through a window in the front side-wall of the cascade, by reflecting it from the diffusely reflecting back side-wall, and by recording the reflected light after it has passed between the blades and back out the window. Because of the blades and other restrictions on access, there is a narrow angle for shadow-free illumination of the interblade passages. It is difficult to avoid recording holograms of the reflections from the window and blades. These reflections may be particularly destructive to heterodyne holography, since their spurious signals can cause systematic phase errors.

Holographic interferometry in wind tunnels such as the flutter cascade requires a double-pulse, Q-switched laser. The laser available for implementing holography in the nine-blade flutter cascade at NASA Lewis is a frequency-doubled Nd:YAG laser, which is optimized to operate at 20 double exposures/sec. The exposure separation can be varied from about 3 to 100 μs. Other suitable lasers would be the ruby laser and possibly the alexandrite laser.

An additional requirement of the heterodyne techniques is the ability to change reference beams between exposures. Ruby lasers, intended for combining holographic interferometry with moire, are available commercially with beam-direction switching capability. For an existing laser such as the Nd:YAG laser in the flutter cascade, a beam switch can be constructed from a Pockels cell and a polarization sensitive beam splitter. A half-wave plate is used after the beam splitter to rotate the polarization of one of the two beams by 90°, so that the speckel patterns of the two holograms are correlated.

A requirement for successful use of diffuse-illumination heterodyne holographic interferometry is to be aware of its systematic and random sources of error. These errors are determined by alignment, by spurious time-varying fringe patterns, by differences in wavelength between the lasers used for recording and reconstruction, and by the electronics used for detection and measurement of the time-varying fringe pattern. There is an additional requirement for a good reference for measuring the relative interferometric phase of the fringe pattern. The random and systematic sources of error are reviewed next. These errors can easily reduce the accuracy of heterodyne holographic interferometry by a factor of 2 to 10.

ERRORS IN DIFFUSE-ILLUMINATION HETERODYNE INTERFEROMETRY

Dändliker and his colleagues have outlined the requirements for dual-reference beam, diffuse-illumination holographic interferometry in several publications.[1-3,21] These papers cover structural analysis, but they are equally applicable to fluid density measurements. The most important points based on our experience are summarized below. Good discussions, with a few errors, are found in Dändliker's publications.

There are two distinct reference waves R_1 and R_2 and two distinct object waves O_1 and O_2 corresponding to the two exposures of the double-exposure hologram. During reconstruction, the frequency of R_1 is shifter relative to the frequency of R_2. Even for linear recording, there is a multitude of time varying interference patterns. To avoid detecting interferences due to the zero-order terms of the hologram, it is essential to satisfy the off-axis-reference-wave criterion, as in Fig. 2. This criterion must be satisfied for any object which is recorded, and every practical effort should be made to avoid illuminating extraneous objects. Even then, care should be exercised to assure that the detectors doe not see reflected zero-order light. Very small spurious signals will cause significant periodic phase errors.

If detection of the zero-order terms is avoided, then the remaining reconstructed waves that can be detected are:

$$R_1R_1^*O_1 \exp(j\omega_1 t) \qquad R_2R_2^*O_2 \exp(j\omega_2 t)$$

$$R_1R_2^*O_1 \exp(j\omega_2 t) \qquad R_1R_2^*O_2 \exp(j\omega_1 t)$$

$$R_1R_2O_2^* \exp(j\omega_1 t) \qquad R_1R_2O_1^* \exp(j\omega_2 t)$$

The waves in the first row are the reconstructions of interest, and do not overlap the reconstructions in the third row, if the reference beams originate from the same side of the diffuser. Overlap with the waves in the second row is avoided by choosing an angle between the reference beams greater than the angular diameter of the diffuser

(Fig. 2), where the diffuser is assumed to be the only object recorded. However, as discussed later, said overlap can be tolerated. The consequences of overlap with these cross reconstructions are a loss of accuracy, but an increase in the tolerance to misalignment.

If the time-varying interference between the waves in the first row is the only signal detected, then that signal is proportional to

$$2\mathrm{Re}[R_1R_1^*R_2R_2^*O_1^*O_2 \exp(j\omega t)]$$

where $\omega = \omega_2 - \omega_1$. If $\Delta\phi$ is the phase difference or interference phase between the two object waves, then the signal varies as $\cos(\Delta\phi + \omega t)$.

If there is a negligible decorrelation between the speckle patterns of the two exposures, and if the above signal can be reconstructed exactly, then the accuracy depends only on the electronics for measuring the interference phase. But any misalignment of the hologram relative to the reference beams, any change in the wavelength of the laser beam, or any misalignment of the reference beams themselves introduces both random and systematic phase errors. The nonlinear nature of the hologram recording process also introduces systematic phase errors.

The proper geometry for imaging the fringe pattern is shown in Fig. 3. The imaging lens is shown placed directly against the hologram. This choice of the lens position eliminates systematic errors, assuming no overlap of the cross reconstructions and neglecting the contributions of the nonlinear terms in the hologram. But the random phase error remains.

If the alignment of the reference beams for reconstruction is perfect, and if the fluid-induced interexposure decorrelation of diffuser speckel patterns is negligible, then each light ray can be treated as unchanged between the two exposures. If the reference beams are misaligned prior to reconstruction, each ray from the reconstructed image from the double-exposure hologram of the diffuser is split into a diverging pair of rays at the hologram as shown in Fig. 4. This divergence results in a lateral shift of the two reconstructions of the diffuser and decorrelation of their speckle patterns. The diverging rays also produce misalignment fringes on the hologram, and the elimination of these fringes can be used for realignment.

If the angle between the diverging rays is α, then the lateral shift of the speckle patterns in the image plane of the lens in the paraxial approximation is given by

$$u = \alpha d \tag{20}$$

where d is the distance of the image of the fringe pattern. If the diameter of the lens used to image the fringe pattern is D, then the fringe contrast is multiplied by a factor

$$\gamma = \frac{2J_1[\pi\alpha D/\lambda]}{\pi\alpha D/\lambda} = \frac{2J_1[\pi Du/(\lambda d)]}{\pi Du/(\lambda d)} \tag{21}$$

The number of misalignment fringes within the aperture of the lens is given by

$$n = \alpha D/\lambda \tag{22}$$

A more serious effect of decorrelation is a random phase error given by the expression

$$\delta\phi = \left[\frac{(1 - \gamma^2)}{2\gamma^2(N + 1)}\right]^{1/2} \tag{23}$$

where N is the number of speckles within the aperture of the detector used to make the phase measurment. For perfect alignment ($\gamma = 1$), there is no phase error. But, a small amount of speckle pattern decorrelation requires a large number of speckles and a correspondingly large detector to compensate.

The above error is reduced by minimizing the number of misalignment fringes in the lens aperture or by minimizing the frequency of those fringes. The spatial frequencies of the misalignment fringes at the hologram are given by

$$f_x = (1/2\pi)][\Delta k_{2x} - \Delta k_{1x}] \tag{24}$$

$$f_y = (1/2\pi)[\Delta k_{2y} - \Delta k_{1y}] \tag{25}$$

where the reference beams are misaligned by Δk_1 and Δk_2, respectively. Misalignment occurs because of a difference in wavelength between the recording and reconstruction beams, because of a change in the included angle between the reference sources, and because of rotation of the hologram about its x_H, y_H, and z_H axes.

If the reference sources are in the x_H, z_H plane, if the reference beams are approximately collimated, and if the hologram is in the x_H, y_H plane, the various sources of misalignment result in the following fringe frequencies:

change $\Delta\lambda$ in wavelength

$$f_y = 0 \quad f_x = (\Delta\lambda/\lambda^2)\,[\cos\theta_{x1} - \cos\theta_{x2}] \tag{26}$$

Symmetrical change $\Delta\theta$ in included angle

$$f_y = 0 \quad f_x = (\Delta\theta/\lambda)\,\sin\left[\frac{\theta_{x1} + \theta_{x2}}{2}\right]\cos\left[\frac{\theta_{x1} - \theta_{x2}}{2}\right] \tag{27}$$

rotation $\Delta\alpha$ about the x-axis

$$f_y = (1/\lambda)[\cos\theta_{z2} - \cos\theta_{z1}]\,\Delta\alpha \quad f_x = 0 \tag{28}$$

rotation $\Delta\beta$ about the y-axis

$$f_y = 0 \quad f_x = (1/\lambda)[\cos\theta_{z1} - \cos\theta_{z2}]\,\Delta\beta \tag{29}$$

rotation $\Delta\gamma$ about the z-axis

$$f_y = (1/\lambda)[\cos\theta_{x1} - \cos\theta_{x2}]\,\Delta\gamma \quad f_x = 0 \tag{30}$$

where $\cos\theta_{x1,2}$, $\cos\theta_{y1,2}$, $\cos\theta_{z1,2}$ are direction cosines of the reconstruction rays relative to the hologram coordinate axes.

A change in wavelength can be compensated by a change in included angle or by rotation about the y-axis.

If there is a large angle between the two reference beams, the required alignment accuracy is high. The best results are achieved when the included angle is large enough to prevent overlap with the cross reconstructions. But the required alignment accuracy may be impractical for transferring the hologram from a test cell to a readout station.

The sensitivity to misalignment can be reduced substantially for Eqs. (26) and (28) to (30) by choosing a very small angle between the reference beams. For a small enough angle, the interference between the reference beams can be viewed and used to set the included angle precisely. The sensitivity to misalignment is reduced enough that film can be used rather than glass plates to record the hologram.

The costs of overlapping the cross reconstructions with the reconstructions of interest are increased systematic and random errors. To avoid a periodic systemmatic error, pairs such as

$$R_1{}^*R_2O_1\,\exp[j\omega_2 t] \text{ and } R_1{}^*R_1O_1\,\exp[j\omega_1 t]$$

must be decorrelated. The magnitude of decorrelation is determined by Eq. (21), where α is now the angle between the two reference beams, and $\alpha D/\lambda$ is the number of reference-beam fringes in the lens aperture. It is desirable to have the voltage produced by any signal at the heterodyne frequency at least 20 dB less than that contributed by the direct interference of O_1 and O_2.

Even if the above decorrelation is adequate, the overlapping speckel patterns contribute an additional random phase error given by

$$\delta\phi = \left[\frac{5}{2(N+1)}\right]^{1/2} \tag{31}$$

where N is the number of speckles in the detector aperture. More than 10^4 speckles are required for a phase error less than 1°. Also, the overlapping reconstructions reduce the fringe contrast.

Another possible source of error, discussed thoroughly by Dändliker,[3] is the nonlinear response of the hologram recording medium. The periodic error produced by this effect is minimized by controlling the parameters that affect linearity (beam ratio, exposure, processing) and by eliminating from the hologram all object waves that do not originate from the changing part of the object.

The implementation of time-average holography for flow visualization involves fewer considerations as discussed in the next section.

IMPLEMENTATION OF TIME-AVERAGE HOLOGRAPHY FOR FLOW VISUALIZATION

Objective

The main objective is to use time-average holography to improve the three-dimensional flow-visualization effect associated with fringe localization. A second objective is to increase the quantitative capabilities of flow visualization based on diffuse-illumination holographic interferometry over those available from the double-exposure method.

One goal eventually is to evaluate time-average holography in the nine-blade flutter cascade mentioned previously. The double exposure holograms recorded of the flows in that cascade show so many flow features that it is at times difficult to isolate them. It is expected that time-average holography with frequency modulation of the reference-beam will allow the fringe contrast of a flow-feature of interest to be enhanced relative to that of other flow features.

PROPERTIES AND REQUIREMENTS

Time-average, diffuse-illumination, holographic interferometry for flow visualization does not differ significantly from time-average holography for the visualization of vibrational modes.[5,15] Furthermore, the flow-visualization effect depends on fringe localization, just as it does for double-exposure, diffuse-illumination, holographic interferometry.

When the time and spatial dependences of the variation of phase can be separated as in Eq. (17), the fringe contrast and fringe localization depend on the spatial part $\phi_r(r_H)$. If the reference beam is modulated as given by Eq. (18), then localization is given by Eqs. (14) and (15), with ϕ_r and γ_r substituted for $\Delta\phi$ and $\Delta\gamma$, respectively. The fringe contrast is determined by the so-called characteristic function, which for separable flows is proportational to Eq. (19). For comparison, the characteristic function for vibrational analysis is proportational to the familiar zero-order Bessel function of the first kind.

For $\gamma_r = 0$ the characteristic function and fringe contrast depend on $\phi_r T/2$. For example, for a two-dimensional flow field, which varies with x,y in a test section of length L along the z-axis, the argument of the characteristic function is given by

$$\phi_r T/2 = \frac{\pi}{\lambda} GLT \frac{\partial \rho}{\partial t} (x,y,t) \tag{32}$$

for rays parallel to the z-axis.

As stated, the potential advantage of time-average holography over double-exposure holography is the ability to use frequency shifts of the reference beams to transfer the highest contrast (brightest) fringe to the flow feature of interest. For Eq. (32), the required circular frequency shift for such a transfer is given by.

$$\omega = \gamma_r = \frac{2\pi}{\lambda} GL \frac{\partial \rho}{\partial t} (x,y,t) \tag{33}$$

A map of the required ω versus position is of course a map of $\partial\rho(x,y,t)/\partial t$.

The only other significant point to note in implementing time-average holography is that its sensitivity, in a certain sense, is one half that of double-exposure holography. For double-exposure holography and the two-dimensional flow of Eqs. (32) and (33), the first fringe minimum (dark fringe) occurs for

$$\frac{2\pi}{\lambda} GLT \frac{\partial \rho}{\partial t} = \pi \tag{34}$$

whereas the first fringe minimum in time-average holography requires that Eq. (34) equal 2π.

The major difficulty in implementing time-average holography for internal transonic flow visualization is to acquire a suitable laser system. Double-exposure holography in the above-mentioned transonic flutter cascade has required exposure separations ranging from 15 to 100 μs. Time-average exposures ranging from 30 to 200 μs would be required for the same sensitivity, assuming no frequency shift of the reference beam.

The long-pulse, flashlamp-pumped, dye laser seems to be the best choice. This laser produces smooth pulses having good beam quality and adequate energy in the required pulse-length range. The major remaining problem is to achieve a narrow enough spectroscopic line-width for adequate temporal coherence and convenient holography.

The actual execution of the beam modulation techniques involves a number of experimental steps, test, evaluations, and preliminary results. These are discussed in the next sections.

EXPERIMENTAL AND DEVELOPMENTAL RESULTS

Expectations and Approach

Dändliker has claimed accuracies for diffuse-illumination heterodyne interferometry of 1/1000 fringe, which corresponds to a phase-measurement accuracy of better than 0.4°. With great care, this accuracy can be achieved in a laboratory. Light must be detected from the primary reconstructions O_1 and O_2 only. The images must be bright, the fringe contrast high, and the alignment for reconstruction very good. The effects of path fluctuations between the reference beams must be minimized, so the reference signal is derived from the fringe pattern itself.

A more realistic expectation is 1/300 fringe, particularly if overlapping cross reconstructions are to be tolerated for ease of alignment and reduced alignment sensitivity.

If the reconstructed images are not bright, if alignment and fringe contrast are poor, or if there are extraneous signals at the frequency offset, then the accuracy can easily drop to 1/100 fringe.

Because of the multiple random and systematic errors that affect accuracy, our approach is to evaluate a heterodyne holography setup in the test cell, but with a flow field or phase object that is both known and repeatable. We use a so-called gas-flow simulator.[22]

Flow Simulator

The flow simulator is a large crystal of KD*P. The crystal, Fig. 5, has 50 by 50 mm faces, which are perpendicular to the optic axis and are separated by 30 mm. Electrodes, 10 mm wide and 50 mm long, are attached to the 50 by 50 mm faces at 4 parallel edges. The actual crystal is held in a mount, where it is submerged in Pockels cell fluid. The two parallel 30 by 50 mm faces are accessible through windows for allowing light to pass through the crystal. Light polarized perpendicular to the optic axis experiences refractive index changes when voltages are applied to the electrodes. The double-exposure holograms compare voltage and no-voltage conditions.

Figure 6 shows the infinite-fringe patterns which result when voltage is applied to electrodes 2 and 4 with electrodes 1 and 3 grounded. The fringe pattern is quite sparse, and its accurate measurement is a good test of the fringe interpolation capability of heterodyne interferometry. The laser illumination has passed through a diffuser before entering the flow simulator.

The flow simulator has been used by Decker and Stricker to compare heterodyne holographic interferometry with conventional finite-fringe holographic interferometry and with heterodyne moire deflectometry.[4] Data from the report is shown in Fig. 7, together with predicted error ranges corresponding to various random fringe-measurement errors. The ordinate of Fig. 7 is the numerically evaluated first derivative of the interference phase, converted to a refractive index derivative by assuming a two-dimensional refractive-index field. It is appropriate to display the derivative of the measurements, since derivatives and differences of the interference phase are required for three-dimensional flow analysis. The graph represents a horizontal scan midway between the 50 by 50 mm faces. The derivatives are determined with central differences with data points separated by 1 mm, and with a 2 mm optical gauge length. That is

$$\Delta\phi_i' = \frac{\Delta\phi_{i+g/2} - \Delta\phi_{i-g/2}}{g} \tag{35}$$

where $g = 2$mm.

The optical setup used to record, reconstruct, and read out the hologram is shown schematically in Fig. 8. Except to remove the hologram and process it, the setup was not disturbed. The 514.5 nm line of the argon-ion laser was used for recording and for reconstruction. The frequency offset was produced with an acoustooptic frequency shifter. The time-varying fringe pattern was detected using two 0.75 mm diameter optical fibers routed to photomultipler tubes. The phase was measured using a dual-phase lock-in amplifier, with the amplified output of one photomultipler used as a reference. The other fiber was translated, and its position measured using a laser interferometer. The lens diameter D was 5.1 cm, and the fringe pattern was imaged at a distance d of 48.3 cm.

The predicted error ranges, shown superimposed on Fig. 7 are of interest in the next section of this report. The ranges show the predicted scatter of the data, should various random fringe-measurement errors occur. Each range is associated with plus or minus a particular value of the fringe interpolation accuracy, and it is seen that the scatter is 50 percent of the general level of the gradient of the refractive index at 1/100 fringe.

As summarized next, the flow simulator was used to investigate possible reference-beam geometries for heterodyne holographic interferometry in the flutter cascade.

Reference-Beam Geometry for a Flutter Cascade

The reference-beam optics were placed together with the flow simulator on a vibration isolation table. The optics consisted of a polarization sensitive beam splitter, a half-wave plate in one beam, an acoustooptic frequency shifter in the other beam, various alignment pinholes and spatial filter assemblies, and a glass-plate holder with precision x,y and y-axis rotation adjustments.

The more desirable wide-angle separation between reference beams was tested first, where the mutual angle was about 7°, and the mean angle was about 45°. The holograms were all recorded at the same flow-simulator settings: 5 kV on electrodes 2 and 4 with electrodes 1 and 3 grounded. The holograms were recorded at 496.5 nm and reconstructed at 514.5 nm, a difference of 18.0 nm. Unless an argon-ion pumped dye laser is used for readout of the holograms recorded with the Nd:YAG laser, those holograms will be recorded at 532 nm and reconstructed at 514.5 nm, a difference of 17.5 nm.

The reference beams were collimated to maintain a constant angle across the hologram. The change in wavelength was compensated for by rotating the hologram about the y (vertical) axis (see Eqs. (26) and (29)). This rotation and the xy adjustments were used to eliminate the misalignment fringes and to maximize the fringe contrast. The fringe pattern was formed at a distance of 48 cm from a 2 cm diameter lens, placed in contact with the hologram. The electronic reference was derived from the fringe pattern itself.

The change in wavelength from recording to reconstruction resulted in a small but noticeable difference. The tolerance of this setup to misalignment followed by realignment was also tested.

A general conclusion is that the wide-angle geometry is feasible, but probably practical only if the holograms are recorded and reconstructed in the test cell. Another possibility is to design and construct identical hardware for the test cell and the readout station, or to construct a portable reference-beam, glass-plate magazine to be transported back and forth. Attempts to use the wide-angle geometry with film were not successful.

The small-angle geometry with overlapping reconstructions was tested next. The same beam switch was used as before, but the reference beams were made nearly coaxial after passing through the half-wave plate and frequency shifter, respectively. The beams were then diverged through a single microscope objective. The mutual angle was set by measuring the separation of the fringes produced by the interference of the two reference beams. Holograms were recorded for various mutual angles varying from 25 to 250 μrad. The only other change in technique was to derive the electronic reference from the interference pattern formed between the two reference beams; the overlapping cross-reconstructions reduce the contrast of the measured fringe pattern and the quality of the electronic reference derived from it.

Vivid examples of the random and systematic phase errors discussed above were easy to generate with this geometry, although the errors were never worse than 1/100 fringe. Results of 1/300 fringe or better required the cross-reconstruction decorrelation associated with at least 10 reference-beam fringes in the lens aperture. The full 5 cm diameter of the imaging lens was used to minimize the random phase error of Eq. (31). Holograms were recorded at 514.5 nm and reconstructed at both 488 nm and 514.5 nm, a difference of 26.5 nm. Fortunately, only minor alignment was required, even after the wavelength change: the reference-beam fringes made it difficult to observe misalignment fringes.

For comparison with Fig. 7, Fig. 9 presents measurements made at 488 nm. The included angle was 100 μrad. Figure 10 presents data measured at 514.5 nm for an included angle of 250 μrad. The lens was close to, but not in contact with, the hologram when these measurements were made.

Film was also used successfully at the small mutual angles, although the best accuracy was only 1/150 fringe. The emulsions used, however, were not the optimum emulsions for the argon-ion laser or for the large average reference-beam angle. Film offers the possibility of higher hologram recording rates or fast processing in the test cell.

The narrow-angle geometry proved fairly easy to use and will be selected at least for the initial work in the flutter cascade. The flow simulator will be built into the measurement system, so that the performance of the system can be tested and checked periodically.

The status of the time-average-holography project is summarized next.

LASER SYSTEM FOR TIME-AVERAGE HOLOGRAPHY

Figure 11 shows the fringe pattern associated with a time-average hologram of a flame induced flow over a blade. The hologram was recorded with an argon-ion laser. The exposure times required for such holograms are 10's to 100's of milliseconds. The internal flows in a flutter cascade by contrast change significantly in 10's of microseconds.

The specification of a suitable laser for transonic flow visualization in the presence of windows using a reflective diffuser has been discussed in another paper.[14] There is no off-the-shelf laser available for time-average holography in such an environment. The general specifications for such a laser are easy enough to state. There should be at least 50 mJ of polarized light per pulse with a spectroscopic full linewidth at half maximum power around 0.03 cm^{-1}. To make good use of higher energies, narrower linewidths are required. The pulses should be smooth and repeatable from shot to shot. Pulse repetition rates at motion-picture frequencies are desirable to increase data rates. As explained previously, pulse lengths up to 200 μs can be used. The beam should have a smooth profile and a small enough diameter and divergence angle to be controlled conveniently. A wavelength that can make use of the most sensitive photographic emulsions is desirable (610 nm to 650 nm for the KODAK SO 253 emulsion).

Commercially available flashlamp-pumped dye lasers are available with pulse widths out to 400 μs. But, the simultaneous narrowing of linewidth, maintenance of pulse width, and control of beam profile have proven difficult. Still, a laser with adequate properties appears to have been constructed and will be tested.

The test of the performance of such a laser is not difficult. For example, if the laser produces pulses having a full length at half maximum power of 50 μs, then a hologram can be recorded of a structure vibrating in a 20 kHz resonant mode. The results can be compared with those recorded with an argon-ion or helium-neon laser. The linewidth can be measured using an interferometer, or better yet by recording a hologram of a scene with a large scene depth.

CONCLUDING REMARKS

It should be convenient to use heterodyne holographic interferometry to measure the relative flow-density field or properties related to it, if the mutual angle between reference beams is small. At least 10 reference-beam fringes are required in the aperture of the imaging lens and more than 10^4 speckles are required in the detector aperture. The flow simulator can be used to determine the error level of the measurement and to assure that systematic errors do not lead to erroneous conclusions concerning complex flows. It is realistic to expect an accuracy of about 1/300 fringe. Higher accuracies are possible with a large mutual angle, but on-site recording, processing, and readout probably are required. Spurious reflections from windows or blades may have a larger effect on accuracy than some of the error sources discussed in this report. It is possible to use film when the angle between reference beams is small.

Heterodyne holographic interferometry is excellent for automated fringe measurements. An automated fringe measurement laboratory is being constructed at NASA Lewis for structural analysis, and will also be used for flow analysis.

It is expected that the flashlamp-pumped dye laser for time-average holography will be available for evaluation very soon.

REFERENCES

1. Dändliker, R., Eliasson, D., Ineichen, D., and Mottier, F.M. (1976). "Quantitative determination of bending and torsion through holographic interferometry," in The Engineering Uses of Coherent Optics, edited by R. Robertson, Cambridge University Press, Cambridge, England, pp. 99-117.

2. Dändliker, R., Ineichen, D., Eliasson, B., and Mastner, J. (1977). "Quantitative Strain and Stress Determination from Holographic Interferograms," (AD-A048640.)

3. Dändliker, R., (1980). "Heterodyne Holographic Interferometry," in Progress in Optics, Volume 17, edited by E. Wolf, North Holland Publishing Co., New York, pp. 1-84.

4. Decker, A.J., and Stricker, J., (1985). "A Comparison of Electronic Heterodyne Moire Deflectometry and Electronic Heterodyne Holographic Interferometry for Flow Measurements," SAE Paper 851896.

5. Stetson, K.A., (1970). "Effects of Beam Modulation on Fringe Loci and Localization in Time-Average Hologram Interferometry," Journal of the Optical Society of America, Vol. 60, No. 10, pp. 1378-1388.

6. Wilson, A.D., (1970). "Characteristic Functions for Time-Average Holography," Journal of the Optical Society of America, Vol. 60, No. 8, pp. 1068-1071.

7. Stetson, K.D., (1976). "The Use of Characteristic Functions in Concomitant Holographic Vibration Analysis," in The Engineering Uses of Coherent Optics, edited by R. Robertson, Cambridge University Press, Cambridge, England, pp. 123-131.

8. Boldman, D.R., and Buggele, A.E., (1978). "Wind Tunnel Tests of a Blade Subjected to Midchord Torsional Oscillation at High Subsonic Stall Flutter Conditions," NASA TM-78998.

9. Strazisar, A.J., and Powell, J.A., (1980). "Laser Anemometer Measurements in a Transonic Axial Flow Compressor Rotor," in Measurement Methods in Rotating Components of Turbomachinery, edited by B. Lakshminarayana and P.W. Runstadler, ASME, New York, pp. 165-176.

10. Strazisar, A.J., and Chima, R.V., (1980). "Comparison Between Optical Measurements and a Numerical Solution of the Flow Field in a Transonic Axial-Flow Compressor Rotor," AIAA Paper 80-1078.

11. Boldman, D.R., Buggele, A.E., and Michalson, G.M., (1981). "Stall Flutter Experiment in a Transonic Oscillation Linear Cascade," NASA TM-82655.

12. Boldman, D.R., Buggele, A.E., and Decker, A.J., (1982). "Three-Dimensional Shock Structure in a Transonic Flutter Cascade," AIAA Journal, Vol. 20, No. 8, pp. 1146-1148.

13. Howes, W.L., (1984). "Rainbow schlieren and its applications," Applied Optics. Vol. 23, No. 14, pp. 2449-2460.

14. Decker, A.J., (1986). "Evaluation of Diffuse-Illumination Holographic Cinematography in a Flutter Cascade," NASA TP-2593 (to be published).

15. Vest, C.M., (1979). Holographic Interferometry," Wiley, New York.

16. Howes, W.L., and Buchele, D.R., (1952). "A Theory and Method for Applying Interferometry to the Measurement of Certain Two-Dimensional Gaseous Density Fields," NACA TN-2693.

17. Howes, W.L., (1985). "Rainbow schlieren vs Mach-Zehnder interferometer: a comparison," Applied Optics, Vol. 24, No. 6, pp. 816-822.

18. Decker, A.J., (1982). "Fringe Localization Requirements for Three-Dimensional Flow Visualization of Shock Waves in Diffuse-Illumination Double-Pulse Holographic Interferometry," NASA TP-1868.

19. Decker, A.J., (1981). "Holographic Flow Visualization of Time-Varying Shock Waves," Applied Optics, Vol. 20, No. 18, pp. 3120-3127.

20. Decker, A.J., (1984). "Measurement of Fluid Properties Using Rapid-Double-Exposure and Time-Average Holographic Interferometry," AIAA Paper 84-1461.

21. Dändliker, R, and Thalmann, R., (1985). "Heterodyne and quasiheterodyne holographic interferometry," Optical Engineering, Vol, 24, No. 5, pp. 824-831.

22. Weimer, D., (1982). "Pockels-Effect Cell for Gas-flow Simulation" NASA TP-2007.

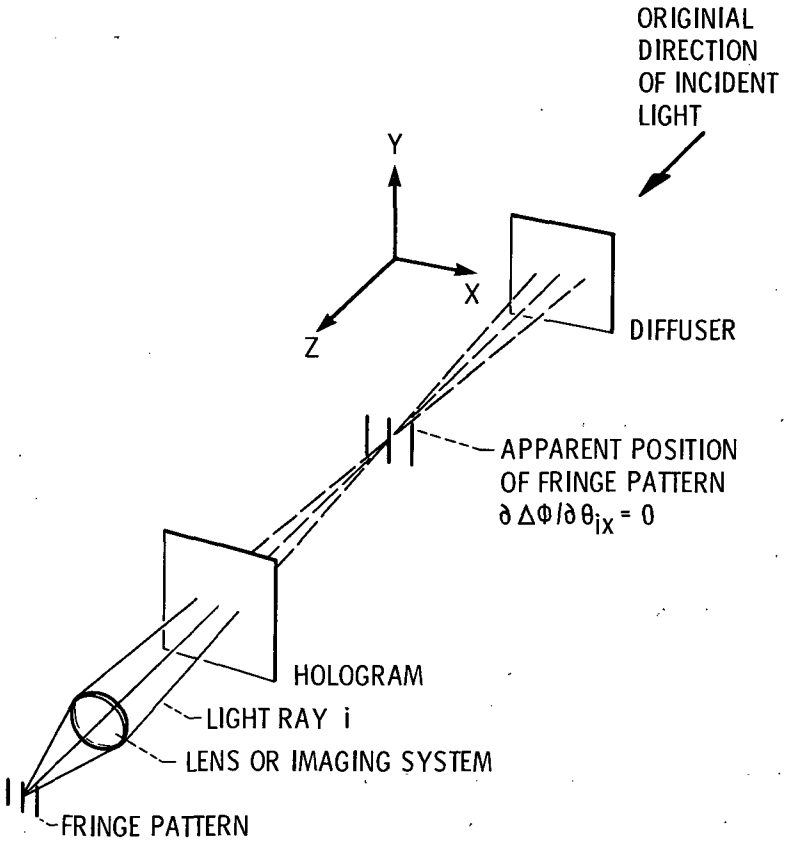

Figure 1. - Imaging a localized interference fringe pattern.

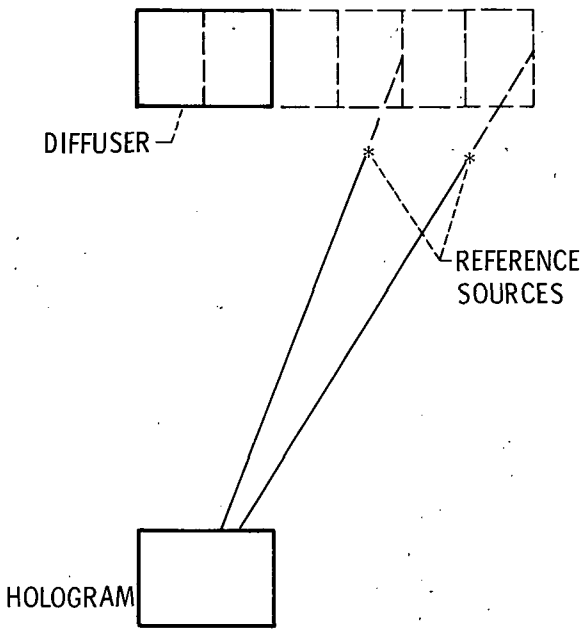

Figure 2. - Minimum reference angles for non-overlapping cross reconstructions and zero-order waves.

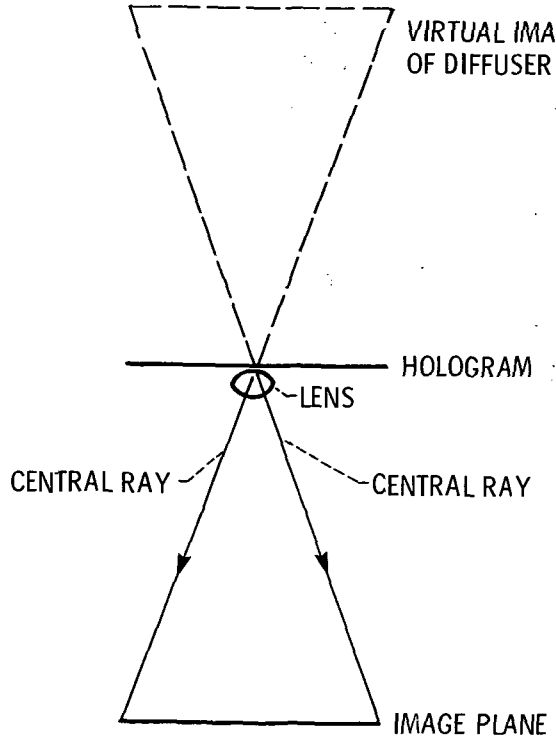

Figure 3. - Proper geometry for imaging fringe pattern in dual reference-beam holography.

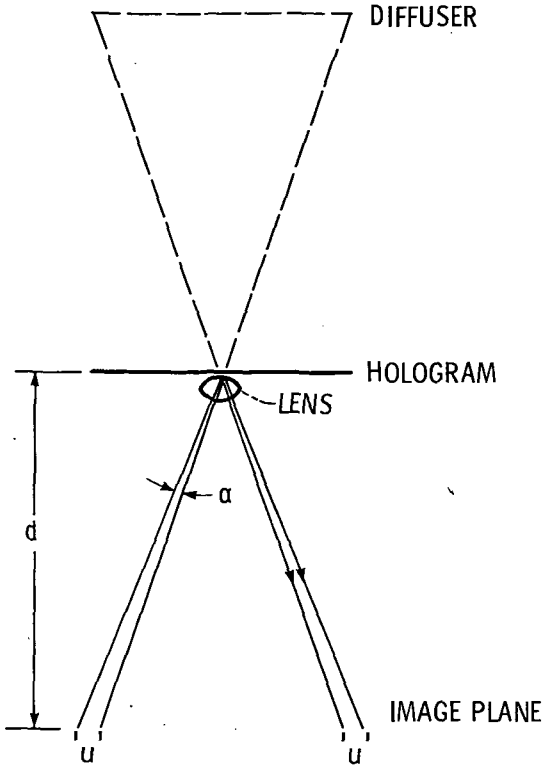

Figure 4. - Splitting of reconstructed rays due to misalignment of reference beams in dual reference-beam holography.

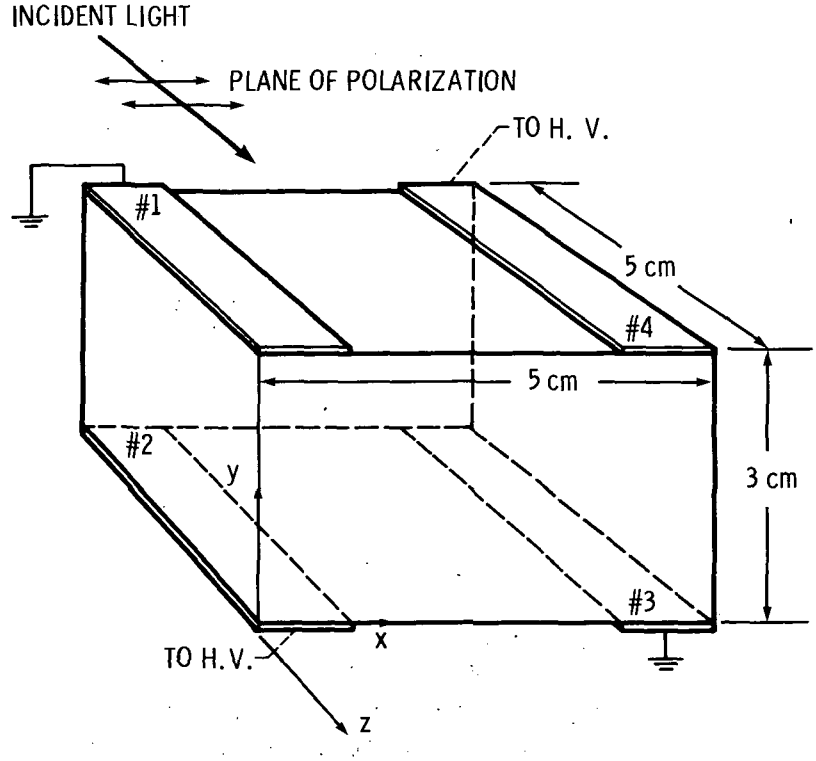

Figure 5. - Flow simulator-crystal of KD*P.

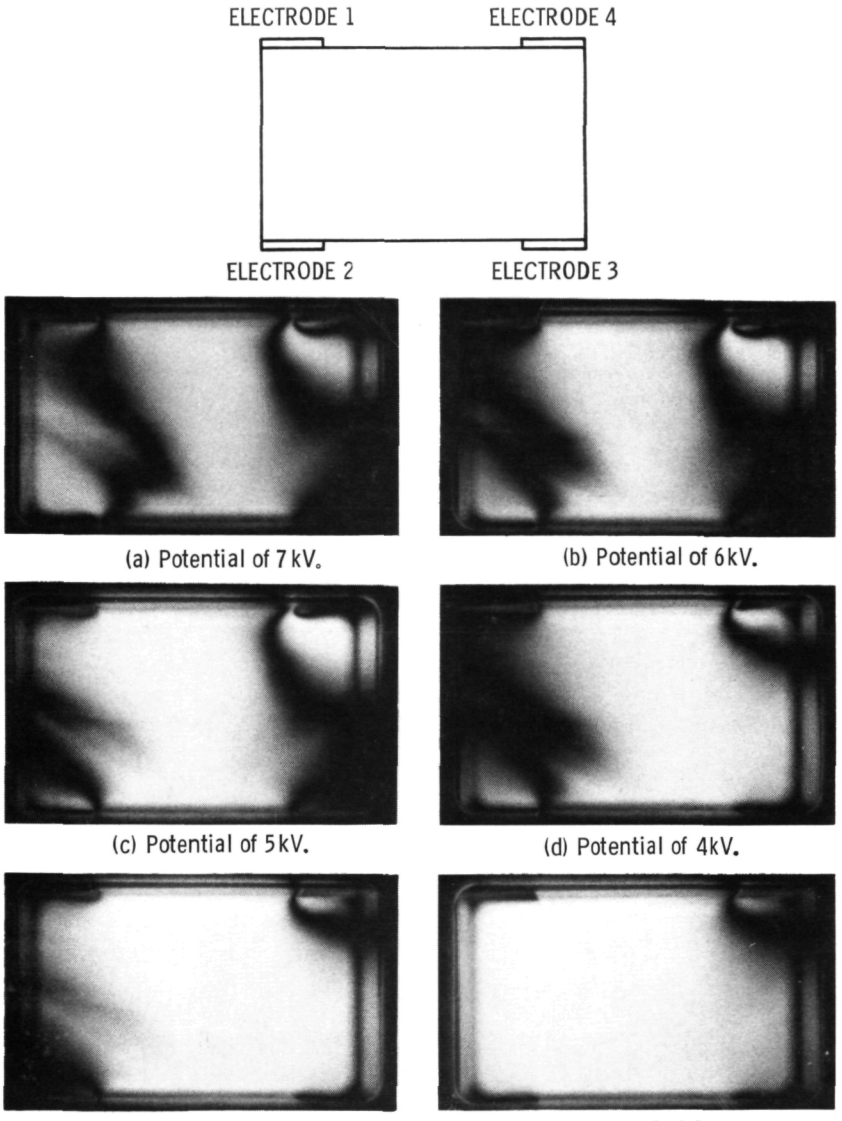

(a) Potential of 7 kV.

(b) Potential of 6kV.

(c) Potential of 5kV.

(d) Potential of 4kV.

(e) Potential of 3kV.

(f) Potential of 2kV.

Figure 6. - Infinite fringe patterns--Pockels flow simulator.

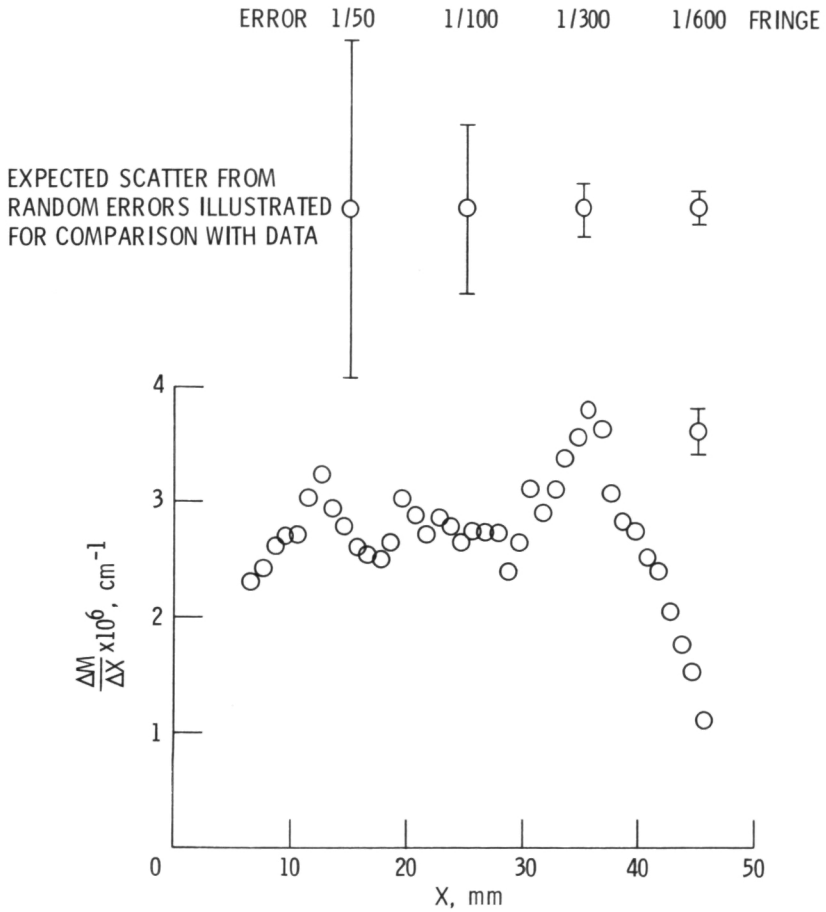

Figure 7. - X-derivative of refractive index of flow simulator, together with expected scatter from various random fringe-measurement errors.

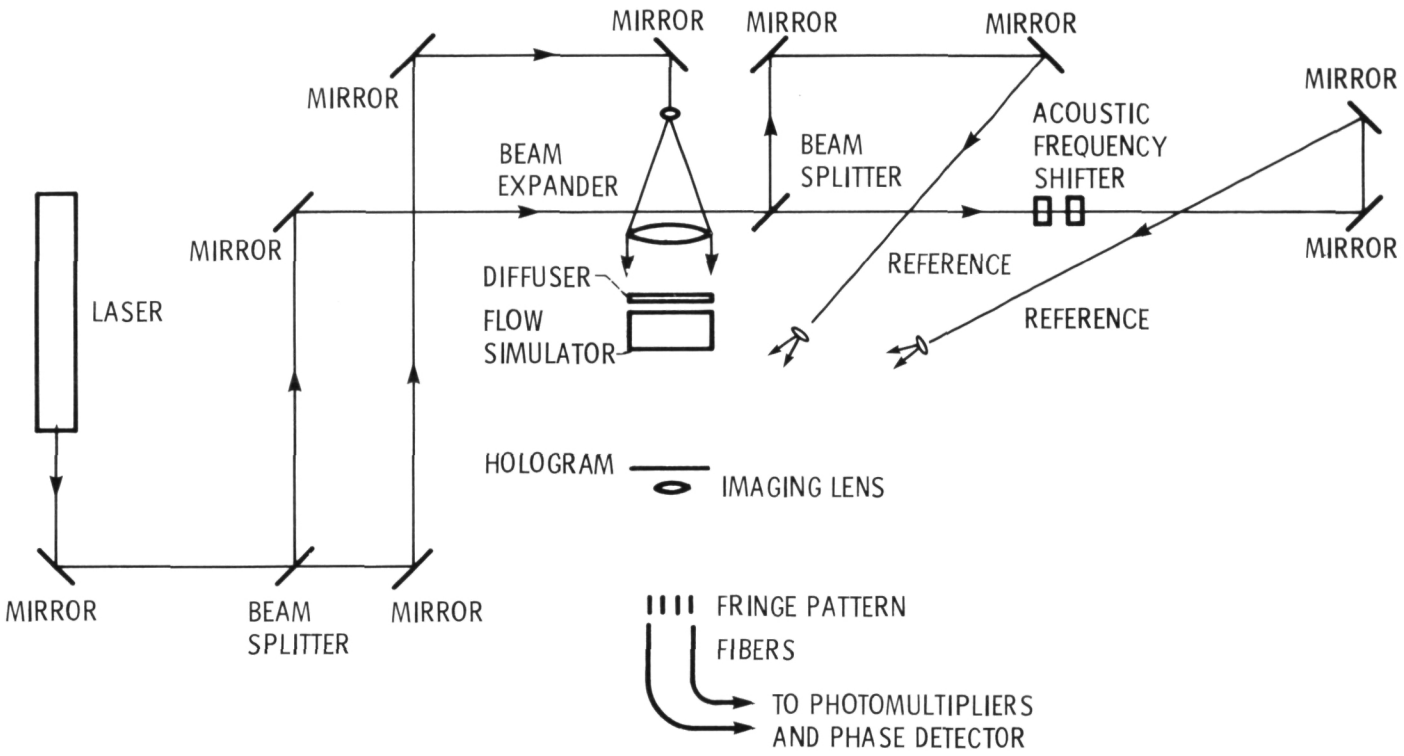

(a) Schematic.

Figure 8. - Electronic heterodyne holographic interferometer.

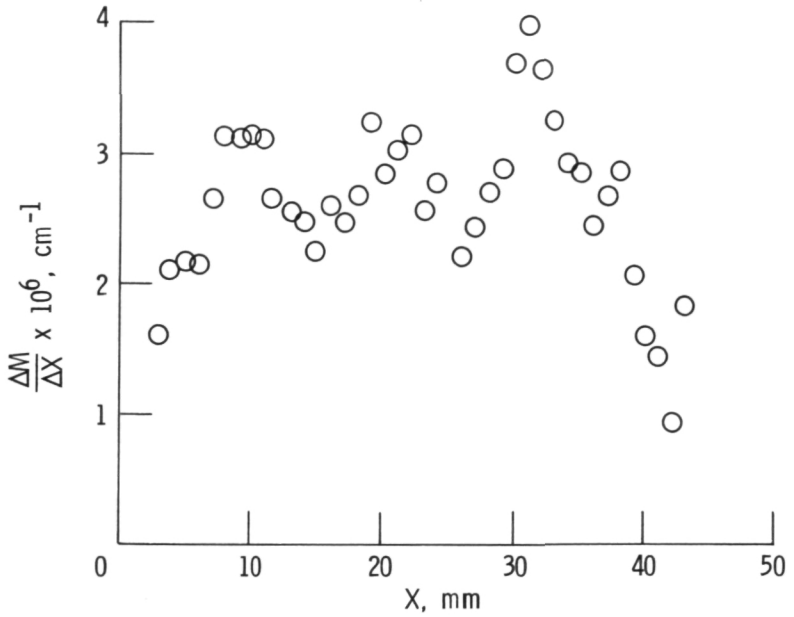

Figure 9. - Flow simulator results: recording wavelength 514.5 mm; reconstruction wavelength, 488 mm, included reference-beam angle 100 μ rad.

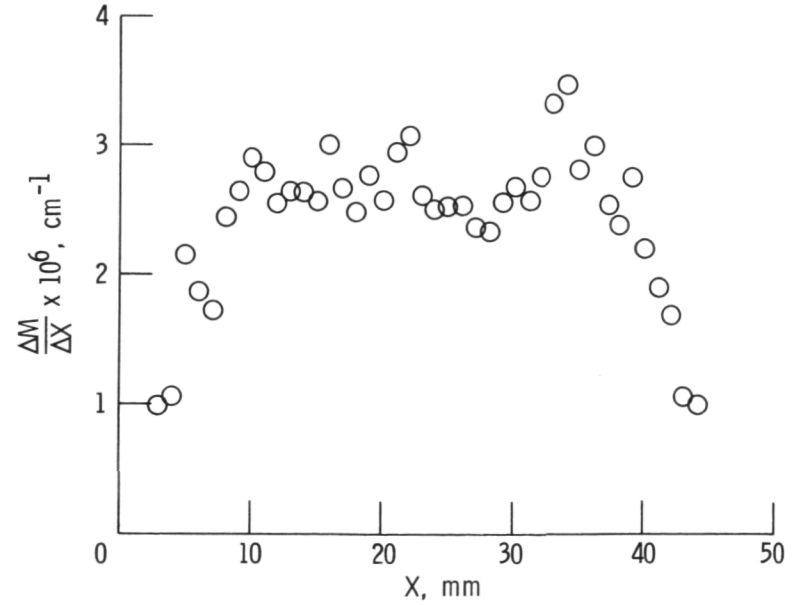

Figure 10. - Flow simulator results: recording wavelength 514.5 mm; reconstruction wavelength 514.5 cm; included reference-beam angle 250 μ rad.

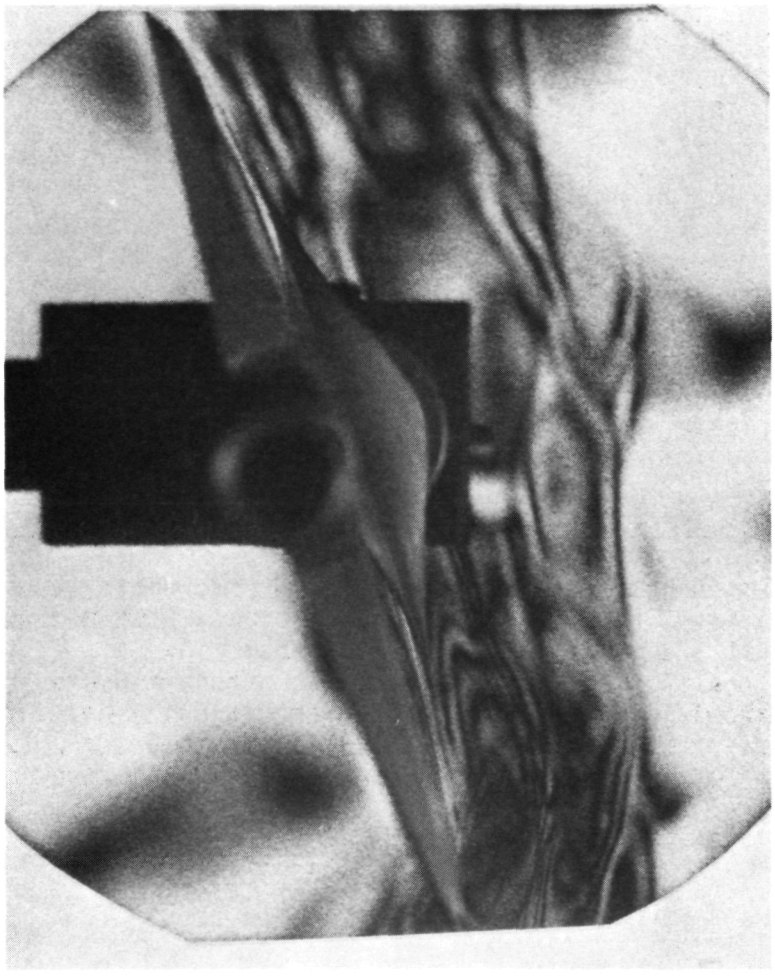

Figure 11. - From time - average hologram of flame - induced flow over blade.

1. Report No.	2. Government Accession No.	3. Recipient's Catalog No.
NASA TM-87306		

4. Title and Subtitle	5. Report Date
Beam-Modulation Methods in Quantitative and Flow-Visualization Holographic Interferometry	6. Performing Organization Code: 505-62-01

7. Author(s)	8. Performing Organization Report No.
Arthur J. Decker	E-3029
	10. Work Unit No.

9. Performing Organization Name and Address	11. Contract or Grant No.
National Aeronautics and Space Administration Lewis Research Center Cleveland, Ohio 44135	13. Type of Report and Period Covered: Technical Memorandum

12. Sponsoring Agency Name and Address	14. Sponsoring Agency Code
National Aeronautics and Space Administration Washington, D.C. 20546	

15. Supplementary Notes

Prepared for the Advanced Instrumentation for Aero Engine Components, sponsored by AGARD, Philadelphia, Pennsylvania, May 19-23, 1986.

16. Abstract

This report discusses heterodyne holographic interferometry and time-average holography with a frequency shifted reference beam. Both methods will be used for the measurement and visualization of internal transonic flows, where the target facility is a flutter cascade. The background and experimental requirements for both methods are reviewed. Measurements using heterodyne holographic interferometry are presented. The performance of the laser required for time-average holography of time-varying transonic flows is discussed.

17. Key Words (Suggested by Author(s))	18. Distribution Statement
Holographic interferometry; Holography; Flow visualization; Heterodyning; Optical heterodyning; Measuring instruments	Unclassified - unlimited STAR Category 35

19. Security Classif. (of this report)	20. Security Classif. (of this page)	21. No. of pages	22. Price*
Unclassified	Unclassified		

*For sale by the National Technical Information Service, Springfield, Virginia 22161

National Aeronautics and
Space Administration

Lewis Research Center
Cleveland, Ohio 44135

NASA